Available online at www.sciencedirect.com

SciVerse ScienceDirect

Acta Materialia 60 (2012) 4160–4171

Acta MATERIALIA

www.elsevier.com/locate/actamat

Serrated flow and stick–slip deformation dynamics in the presence of shear-band interactions for a Zr-based metallic glass

B.A. Sun [a,*], S. Pauly [a], J. Tan [a], M. Stoica [a], W.H. Wang [b], U. Kühn [a], J. Eckert [a,c]

[a] IFW Dresden, Institut für Komplexe Materialien, Helmholtzstrasse 20, D-01069 Dresden, Germany
[b] Institute of Physics, Chinese Academy of Science, Beijing 100190, People's Republic of China
[c] TU Dresden, Institut für Werkstoffwissenschaft, Helmholtzstrasse 7, D-01069 Dresden, Germany

Received 21 September 2011; received in revised form 7 April 2012; accepted 9 April 2012

Abstract

In this paper, shear-band interactions (SBIs) were introduced by a simple method and their effect on the dynamics of shear bands and serrated flow was studied for a Zr-based metallic glass. Statistical analysis on serrations shows that the stick–slip dynamics of interacting shear bands is a complex, scale-free process, in which shear bands are highly correlated. Both the stress drop magnitude and the incubation time for serrations follow a power-law distribution, presenting a sharp contrast to the randomly generated, uncorrelated serrated flow events in the absence of SBIs. Observations on the fracture morphologies provide further evidence and insights into the deformation dynamics dominated by SBIs. A stick–slip model for multiple shear bands with interactions is also proposed and numerically calculated. The results, in good agreement with the experimental results, quantitatively show how multiple shear bands operate and correlate, especially for those with large serrated flow events. Our studies suggest that one serration in the stress–strain curve may correspond to collective stick–slip motions of multiple shear bands for those ductile bulk metallic glasses where a large number of shear bands are observed during deformation.

Keywords: Metallic glass; Serrated flow; Stick–slip; Shear band

1. Introduction

At temperatures well below the glass transition, metallic glasses typically deform inhomogeneously with plastic strain highly localized into thin shear bands [1–3], which is completely different from the dislocation-mediated plasticity in crystalline alloys. Characterizing the shear banding process [4–10] in parallel with theoretical efforts to describe the underlying physical origin [11–16] has been the subject of extensive research in the past decades, and still attracts considerable interest [17], particularly for the case of bulk metallic glasses (BMGs) which have attractive properties such as high strength and large elastic limit, and wide potential applications [18–22]. Focused topics include the structure of shear bands [23–25], the temperature rise of shear bands during deformation, the free volume accumulation or volume dilation within shear bands [4,10,26] and the velocity of propagating shear bands [5,27–29], features which are all indispensable for a full description and understanding of shear band dynamics.

Broadly speaking, a shear band is usually initiated at a local region by some softening mechanism, which has been attributed to the influence of local heating [30–32] or shear dilation (free volume generation) [11–13], or a combination of both [33]. Once triggered, such a shear band will propagate rapidly due to the reduced viscosity or resistance to deformation in its vicinity, leading to catastrophic failure of the glass along the primary shear plane. The macroscopic outcome is almost the zero plastic deformability in tension testing [31], thus limiting the wider application of BMGs. The shear banding process in compression, how-

* Corresponding author. Tel.: +49 351 4659 532; fax: +49 351 4659 452.
E-mail address: b.sun@ifw-dresden.de (B.A. Sun).

1359-6454/$36.00
http://dx.doi.org/10.1016/j.actamat.2012.04.013

ever, does not always have catastrophic consequences. Some BMGs can undergo shear banding in a stable and intermittent manner, which manifests as serrated flow behavior in the plastic regime of stress–strain curves [4]. Similar behaviors are also widely observed in other load-constrained modes such as pop-ins during nanoindentation [34]. The serration process is characterized by repeated cycles of a sudden stress drop followed by reloading elastically. In addition, serrated flow also shows a strong dependence on the strain rate and the temperature [6,9,35]. For example, serrations tend to be suppressed at high strain rates or low temperatures, and disappear at certain critical values [34]. Despite extensive studies, the physical origin of serrated flow as well as its connection to the shear banding process in metallic glasses is still elusive.

In an early study of the compressive behavior of Zr-based BMGs, Wright et al. [4] assumed that each serration was associated with the emission of an individual shear band, and subsequently offered a detailed analysis of the shear-band dynamics. Although the location from which a shear band was emitted was not identified, the assumption of individual shear-band emission has since been widely accepted for interpreting the deformation behavior of BMGs under different loading modes. Based on this viewpoint, Schuh et al. [34] attributed the disappearance of serrations at high strain rates in nanoindentation to the kinetic limitation for shear bands, where a single shear band cannot accommodate the imposed strain rapidly enough at high strain rates, and consequently, multiple shear bands operate simultaneously. Some authors [36] also correlated each serration with the shear-band activity on the surface of deformed specimens based on the observation of rate-dependent shear-band patterns. Recently, the serrated flow in compression was recognized to arise from the stick–slip operation of a single shear band [7–9]. Song et al. [8] found that the regularly spaced striations on the shear surface match well with the serration spacing recorded in the load–displacement curve, and further *in situ* compression experiments also revealed a one-to-one correspondence between the intermittent slidings of the primary shear band and the serrated events. By carefully correcting the experimentally determined displacement jump magnitude during a serration, Maaß et al. have shown that the disappearance of serrations on lowering the temperature was directly linked to the shear-band propagation velocity, and the transition occurred at the temperature for which the shear-band velocity equals the applied cross-head velocity, giving underpinning evidence that flow serrations are caused by intermittent shear-band slidings in BMGs [9].

The stick–slip process of shear banding indicates that the mechanical properties of BMGs (especially plasticity) are not only affected by intrinsic properties such as the glassy structure [37,38] and free volume contents [39], but also by the extrinsic materials properties [15,40] and experimental factors [41,42]. Indeed, Han et al. [40] have shown that the plasticity of monolithic BMGs strongly depends on the sample size and the stiffness of the testing machine. Based on the observations, they proposed a single parameter, called the "shear-band instability index", that governs the critical transition from unstable to stable shear banding as a function of sample size and machine stiffness. In addition, enhanced plasticity may also be a consequence of geometrical constraints during mechanical testing. For instance, after a carefully conducted series of compression tests, Wu et al. [42] found that any deviation from a perfect coaxial alignment of the sample with respect to the compression axis results in a large apparent plasticity. Recently, Cheng et al. [15] also proposed a stick–slip model for the operation of a single shear band, which quantitatively showed that the experimental factors (such as sample size and machine stiffness) can greatly affect the temperature rise in the shear band as well as its sliding speed, thus causing either cold and stable or hot and runway shear banding in BMGs.

Usually, most BMGs fail along a single dominant shear band. Most analyses so far have focused on the instability process of such a single shear band. However, for some ductile BMGs or their composites [43], the deformation proceeds via the simultaneous operation of multiple shear bands, with each band contributing to the plasticity and none of them carrying enough strain to cause catastrophic failure, thus leading to the large plasticity. In such cases, shear bands inevitably interact with each other and thus affect their formation and propagation. A few studies [44–46] have shown that SBIs play an important role in the dynamics of multiple shear bands. However, it is difficult to characterize SBIs due to the fact that shear bands are spatially and temporally generated, and also have a short propagation time. In this study, we introduce SBIs by a simple method and study their effects on the deformation dynamics and serrated flow in a Zr-based metallic glass. A stick–slip model considering SBI is also proposed and calculated, showing how multiple shear bands operate and correlate during a single serration event.

2. Experimental procedures

Alloy ingots with a nominal composition of $Zr_{65}Cu_{15}Ni_{10}Al_{10}$ were produced by arc melting a mixture of pure metals (purity $\geqslant$ 99.5%) in a Ti-gettered argon atmosphere. To ensure compositional homogeneity, each ingot was remelted at least three times. Rod-shaped samples with a diameter of 1.5 mm and a length of about 50 mm were obtained by suction casting into a copper mold. The amorphous nature of the as-cast specimens was examined by X-ray diffraction (XRD, PANalytical X'Pert PRO) with Co K_α radiation and differential scanning calorimetry (DSC, Perkin Elmer DSC7). Specimens about 4 mm long were cut from BMG rods by means of a diamond saw, and then carefully ground into compression specimens with an aspect ratio of 2:1 to an accuracy of ± 5 μm. Uniaxial compression tests were performed with an Instron 5869 electromechanical test system at a constant strain rate of $2 \times 10^{-4}\ s^{-1}$ at room temperature. The strain was mea-

sured by a laser extensometer (Fiedler) attached to the testing machine. Special care was taken to ensure that the two surfaces of test specimens were parallel and orthogonal to the loading axis. For samples tested simultaneously, they were ground together to ensure an identical height. Load, displacement, extension and time were measured and digitally stored at a frequency of 50 Hz (50 data points per second). After deformation, the morphologies of shear bands as well as fracture surfaces were investigated via a high-resolution scanning electron microscopy (SEM, Gemini 1530).

3. Results and discussion

3.1. Introduction of shear-band interactions

When tested in compression, a BMG sample usually deforms by the formation of a single dominant shear band. In such a case, the deformation behavior of BMGs can be described by the stick–slip model of a single shear band [37,17], as shown in the left part of Fig. 1a. The machine–sample system (MSS) is loaded at a slow, constant rate v at time $t = 0$. The stiffness of the machine and the sample is κ_M and κ_S, respectively. The elastic energy stored in the machine and the sample gradually increases during deformation and provides the driving force, $\kappa_M\kappa_S vt/(\kappa_M + \kappa_S)$. Once the driving force exceeds the intrinsic resistance of the band, it will be activated and slide with the vertical displacement, x. When shear band is operated, the elastic energy stored in the MSS will be released, involving the elastic unloading of both the machine and the sample (x_M and x_S, respectively), thus partially relieving the driving force by $\kappa_M\kappa_S x/(\kappa_M + \kappa_S)$ (from $x = x_M + x_S$ and $\kappa_M x_M = \kappa_S x_S$). The governing kinetic equation for the MSS is:

$$\frac{\kappa_M\kappa_S}{\kappa_M + \kappa_S}(vt - x) - \frac{\pi d^2}{4}\sigma_f = Mx'' \tag{1}$$

where d is the sample diameter, M is the effective inertia of the MSS (typically of the order of 10–100 kg [15]), and x'' is the second derivative of x. σ_f is the internal resistance of the shear band, which should be a complex function of the intrinsic properties (free volume content and temperature, see the detailed discussion in Section 3.5). We define the elastic constant as:

$$k = \frac{4\kappa_M\kappa_S}{\pi(\kappa_M + \kappa_S)d^2} = \frac{E}{L(1+S)} \tag{2}$$

where L is the sample height, E is the Young's modulus and S is the shear-band instability index defined as $S = \kappa_S/\kappa_M = \frac{\pi d^2 E}{4L\kappa_M}$ [40]. The springs of machine and sample in the MSS can be simplified into one spring, as shown in the right part of Fig. 1a. Eq. (1) then becomes:

$$[k(vt - x) - \sigma_f]\frac{\pi d^2}{4} = Mx'' \tag{3}$$

Eq. (3) indicates that the shear banding is affected by both extrinsic factors (reflected by k) and intrinsic properties of the glass material (reflected by σ_f). We note that SBIs are not presented in the model above. However, if several samples are tested simultaneously in compression (see Fig. 1b), the operation of one shear band will release the elastic energy of the whole system. Due to the constraint of the cross-head of the testing machine, the elastic energy must be accommodated by the operation of all the shear bands. In this case, we take the average elastic unloading displacement for the sample springs. Thus, the relieving force during the elastic unloading is $\kappa_M\kappa_S\sum x_j/(\kappa_M + n\kappa_S)$, where n is the number of samples, x_j is the displacement of the jth shear band and $\sum x_j$ is the sum over all samples. In this case, the kinetic equation for the system is:

$$\frac{n\kappa_M\kappa_S}{\kappa_M + n\kappa_S}\left(vt - \frac{1}{n}\sum x_j\right) - \frac{\pi d^2}{4}\quad \sigma_{fi} = Mx_i'', i = 1, \ldots n \tag{4}$$

where σ_{fi} is the internal resistance of the ith shear band. Following the same procedure with the model of single shear band, we also define the elastic constant:

$$k_1 = \frac{4n\kappa_M\kappa_S}{\pi(\kappa_M + n\kappa_S)d^2} = \frac{E}{L(1/n + S)} \tag{5}$$

Taking this into Eq. (4) and rearranging the terms, we obtain:

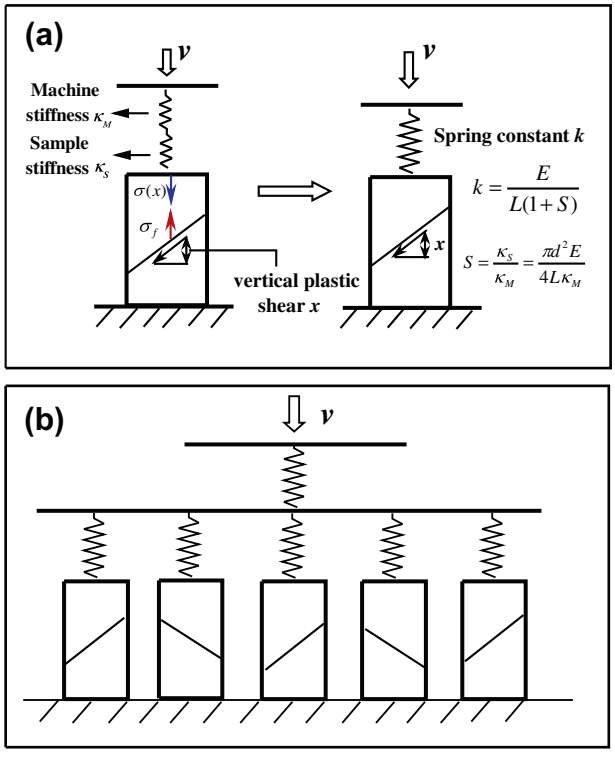

Fig. 1. Schematic diagrams of the stick–slip model for a single sample where only a dominant shear band formed (a) and several samples tested simultaneously (b).

$$\left[k_1(vt - x_i) + k_1\left(x_i - \frac{1}{n}\sum x_j\right) - \sigma_{fi}\right]\frac{\pi d^2}{4} = Mx_i'', \quad i = 1, \ldots n \tag{6}$$

where $k_1(x_i - 1/n\sum x_j)$ can be regarded as the interactions between shear bands. It represents the effect of the operation of the other shear bands on the ith shear band. Thus, the interactions between shear bands is introduced by this simple method, which will significantly affect the dynamics of shear bands during deformation.

3.2. Deformation behavior of BMGs

We start by performing single-sample compression tests (SSTs) and multiple-sample compression tests (MSTs), respectively, and then compare their deformation behavior. For the MSTs, five BMG samples are simultaneously loaded up to the failure of any of them. Fig. 2a and b shows the typical stress–strain and stress–time curves for SSTs and MSTs at the strain rate of $2 \times 10^{-4}\,s^{-1}$, respectively. Both curves exhibit obvious serrated flow in the plastic regime after yielding at about 2% elastic strain. After deformation, all the samples both in SSTs and MSTs failed along a dominant shear band (see the inset in Fig. 2a), verifying our assumption in the models above. The plastic strain before failure in the MSTs can reach 9%, which is much larger than that in the SSTs (5%), suggesting that the shear-banding process is more stable in the presence of SBIs. The results are also consistent with previous studies, which have shown that the formation and interaction of multiple shear bands enhances the plasticity in BMGs [43,47]. Even more interesting is the change of serrated flow behavior after introducing SBIs. As seen from the enlarged segments of the stress–time curves in Fig. 2c, the serrations of the MSTs are much more complex with numerous small stress drops but fewer large ones, compared with the more uniform large serrations in the SST. As serrations arise from the intermittent motion of shear bands, the change in serrated flow behavior indicates a change in shear band dynamics after introducing SBIs. In the following, we will give a detailed statistical analysis of serrations for both curves.

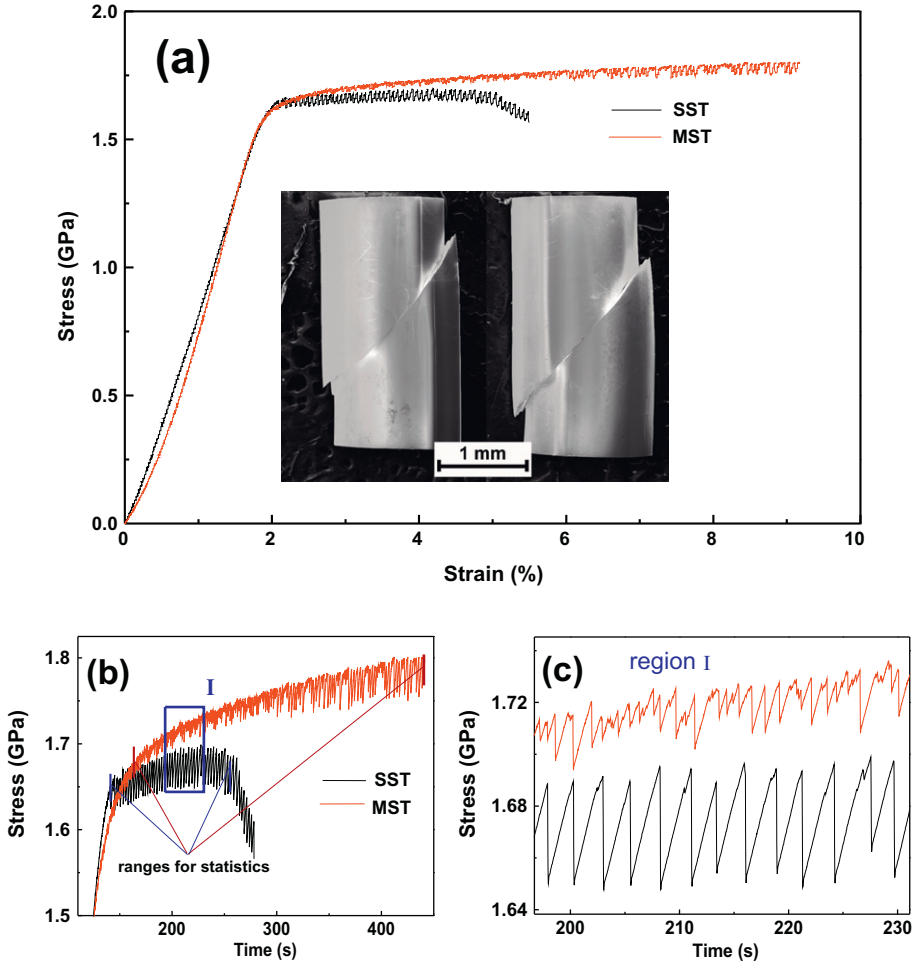

Fig. 2. (a) Compression stress–strain curves for the SST and MST at the strain rate of $2 \times 10^{-4}\,s^{-1}$. The inset shows photographs of the specimen before catastrophic failure: the left for SST and the right for MST. (b) The stress–time curves for the SST and MST, which show the range of statistical analysis. (c) Enlarged view of the region I, showing the serrations of the SST and MST at the same time window.

3.3. Statistical analysis of serrations

As seen in Fig. 3a, the serration process is characterized by repeated cycles of a sudden stress drop followed by an elastic loading part. The sudden stress drop in one serration often corresponds to the rapid shear-band operation, during which the measured shear-band propagation velocity is in the range of 10^{-3}–10^{-2} ms^{-1} [27], which is much faster than the external loading rate ($v_{ch} = 6 \times 10^{-7}$ ms^{-1} in the present study). Thus, the serration process is a typical stick–slip phenomenon characterized by a "stick phase" that usually lasts much longer than the "slip phase", which has been verified by recent studies [9]. Stick–slip dynamics has been observed in a large number of systems ranging in scale from atomically thin film to earthquake faults [48–50].

A effective way to study the underlying process of stick–slip dynamics is to consider the statistics of slip events. We first analyze the distribution of the stress drop magnitude as it has been shown to be proportional to the shear displacement during one serration and thus can be used as a measure of the size of plastic events [46,48]. As shown in Fig. 3a, the stress drop magnitude is taken to be the difference between the maximum and the minimum of each serration denoted by $\Delta\sigma_s$. Before calculating the statistics, a normalization of stress drop magnitude is necessary as the serration size often increases with strain or time, thus, causes a systematic shift of serration amplitude $\Delta\sigma_s$ [46]. The increasing of $\Delta\sigma_s$ with time analyzed from the stress–time curve of the MSTs can be seen in Fig. 4a. The increasing trend may originate from the gradually increasing cross-sectional area of sample during deformation and thus does not reflect the fundamental aspects of shear-band dynamics. As shown in Fig. 4b, using a linear regression fit through the stress drop vs. time diagram, $\overline{\Delta\sigma_s} = f(t)$,

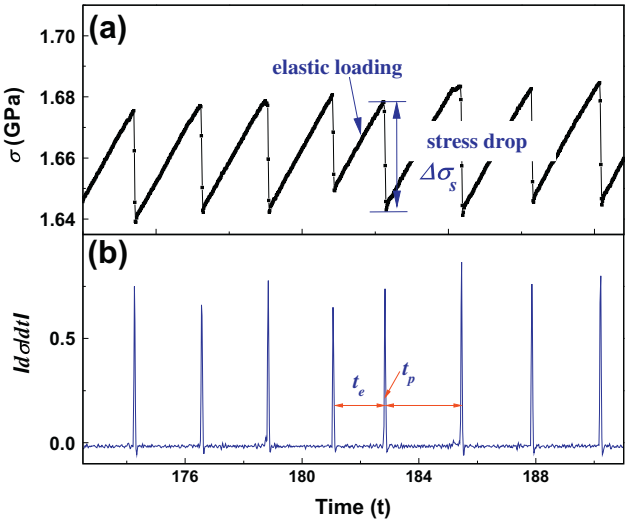

Fig. 3. (a) An example of serrations taken from the stress–time curve of the SST. (b) The absolute derivative of the stress to the time from (a), which shows the incubation time, t_e, and the duration, t_p, of a single serration.

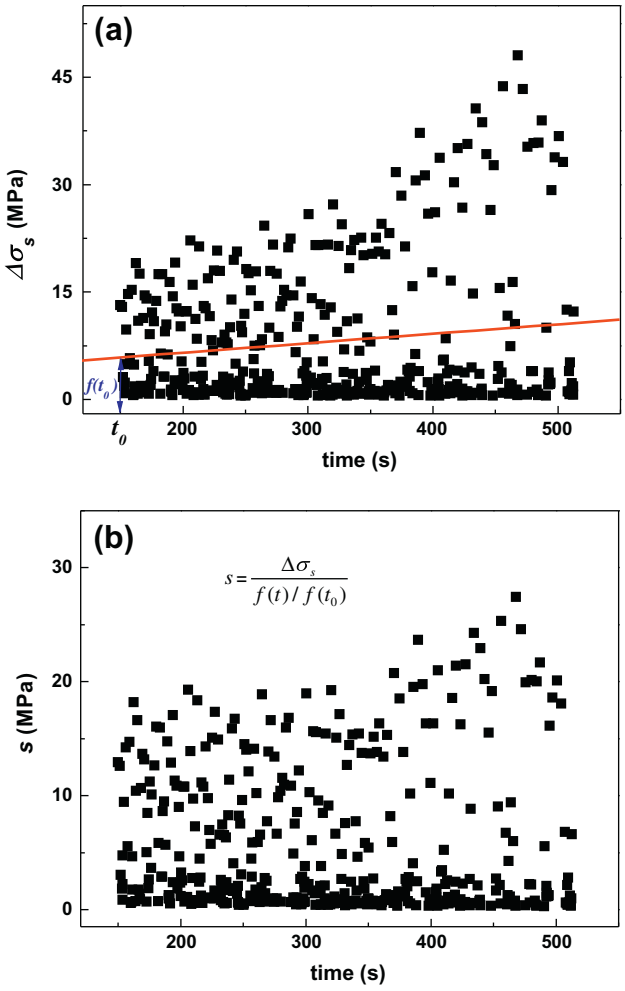

Fig. 4. (a) The stress drop magnitude $\Delta\sigma_s$with time t for the MST. The red line is the average stress drop obtained by the linear regression fit. $f(t_0)$ is also labeled. (b) The normalized stress drop magnitude s with the time t. (For interpretation of the references to colour in this figure legend, the reader is referred to the web version of this article.)

the normalized stress drops, $s = \frac{\Delta\sigma_s}{f(t)/f(t_0)}$, where $f(t_0)$ is the fitted value at the starting time of statistics t_0 (see Fig. 4a), are considered. It is noted that the vibrations of the cross-head of the testing machine will also induce small serrations [44,46]. Generally, these stress vibrations are less than 0.5 MPa [46], and hence the serrations with $\Delta\sigma_s < 0.5$ MPa are not counted in our statistics. In addition, as pointed out by Song et al. [27], the serrations in the initial stage of plastic deformation (the bending part of the stress–time curve) mainly arise from the formation of highly discreted localized shear bands. Thus, we only count the serrations in the stable plastic regime for each curve (labeled in Fig. 2b), as this regime reflects the operation process of the dominant shear band.

The distribution histograms of the normalized stress drops for SSTs and MSTs are shown in Fig. 5a and b, respectively. One can see that the histograms for the SSTs display a peak shape with most stress drops concentrated in the range of 20 MPa $< s <$ 40 MPa (Fig. 5a). This indicates

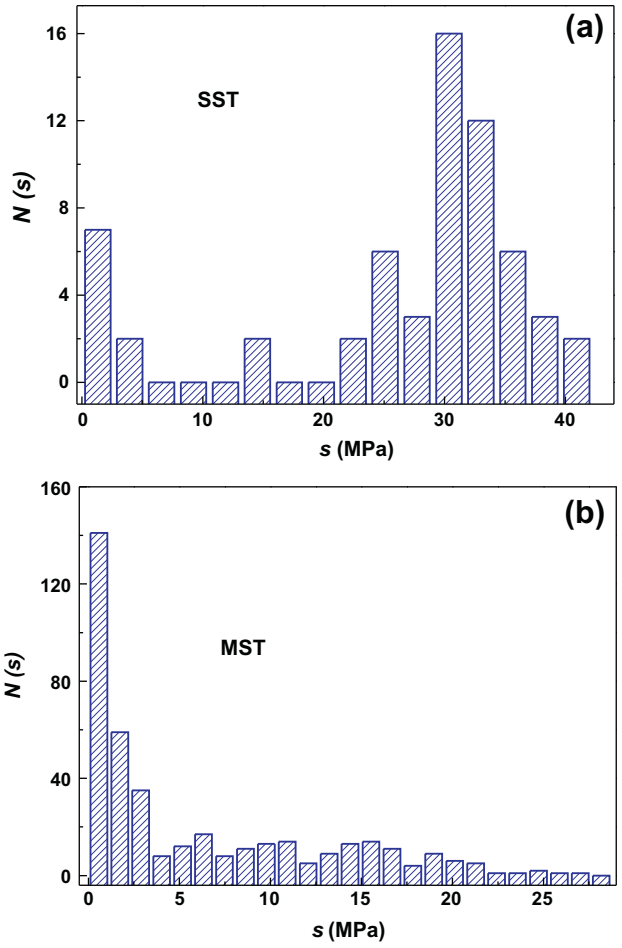

Fig. 5. Numbers of stress drops $N(s)$ vs. the normalized stress drop magnitude s for SST (a) and MST (b).

that the serration size for the SSTs has a characteristic length scale. The peak distribution of stress drops was also observed from the analysis of the Portevin–Le Chatelier (PLC) effect in crystalline allys, which is a well-established example of chaotic stick–slip dynamics arising from the collective pinning and unpinning of dislocations from solute atmosphere [48]. Recently, a time series analysis performed on a brittle BMG by Samah et al. [44] also confirmed the chaotic dynamics of serrated flow, corroborating the similarity between the serrated flow in BMGs and the PLC effect in crystalline alloys [51].

In contrast, the serrations for the MSTs are much more complex and display a monotonically decreasing distribution (Fig. 5b) indicating that the fundamental dynamics of shear banding has changed after the introducing of SBIs. To quantify this, the cumulative probability distribution, $P(>s)$, i.e. the percentage of the serrations with a stress drop larger than a certain value of s, is calculated and plotted in Fig. 6. It can be seen that $P(>s)$ can be well fitted by a power-law distribution with a squared exponential decay function:

$$P(>s) = As^{-\beta} exp\left[-(s/s_c)^2\right] \quad (7)$$

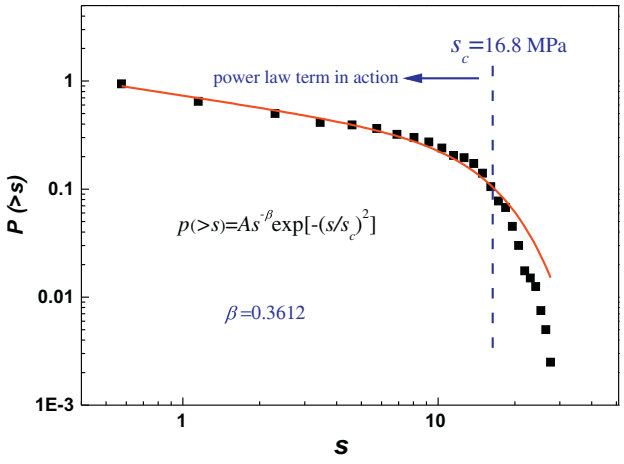

Fig. 6. Logarithmic plot of the cumulative distribution of stress drops $P(>s)$ vs. stress drop magnitude s for the MST.

where A is a normalized constant, β is a scaling exponent and s_c is the cut-off stress drop magnitude. Eq. (7) suggests that the distribution of the stress drops is essentially a power-law relation up to a large value of stress drop magnitude, s_c, where the squared exponential decay factor comes into play. The fitting values for β and s_c are 0.3612 and 16.8 MPa, respectively.

The power-law relation is often an indicator of the self-organized critical (SOC) state in dynamics [52], where the entities constituting the system interact under an external slowing driving force, causing rapid avalanche events once the minimum stable states are reached. The size of avalanches has no characteristic scale, and is only delimited by the finite size of the system. Many complex systems such as earthquakes and sandpiles are found to exhibit SOC behavior [52,53]. Recently, Wang et al. [54] also demonstrated that Eq. (7) holds for the distribution of the elastic energy density of serrations in BMGs, and they have suggested that the dynamics of serrated flow in BMGs is SOC. In our case, the deduction of the SOC from the analysis of serrations should be made with some caution, as the power law alone does not provide unequivocal evidence for it. In addition, the number of shear bands involved in the MSTs is only few ($N = 5$), whereas the SOC is often characterized by infinite (theoretically) degrees of freedom, involving a large number of interacting entities [52]. However, the emergence of the power-law term in Eq. (7) indeed implies that shear bands are highly correlated in the MSTs. They slide collectively due to SBIs in one single serration, causing avalanche-like plastic events. The squared exponential function in the power-law function accounts for the finite size of serration events. The s_c value suggests that there is an upper limit for the size of the system. Thus it is expected that s_c will increase when we used more BMG samples in the MSTs.

To further reveal the underlying dynamics of serrated flow in the presence of SBIs, we also performed statistical analysis of the incubation time for the serrated events, i.e

the elastic loading time, t_e, before the stress drop occurred (Fig. 3b). In avalanche dynamics, the distribution of the incubation times is a signature for the correlation between separate avalanche events [55]. Fig. 7 shows the cumulative probability distribution of the incubation times, $P(>t_e)$, for the SSTs and MSTs, respectively. Apparently, the distribution for the SSTs is well described by a Poisson process, $P(>t_e) = exp(-t_e/\tau)$, with the fitting parameter, $\tau = 1.51$. τ is the rate parameter, which is often regarded as the expected number of events that occur per unit time [56]. The Poisson distribution indicates that serrated events in the SSTs are uncorrelated and randomly generated at a rate of $\tau = 1.5$. In contrast, the distribution for the MSTs follows a power-law relation, $P(> t_e) \sim t_e^{-D}$, with an exponent $D = 2.17$. This behavior indicates that the triggering of serrated events is correlated. In other words, the occurrence of one serration is affected and determined by previous serrations. Thus, in the presence of SBIs, there are correlations not only regarding the operation of shear bands within a serration, but also regarding the occurrence of serrations during the deformation of BMGs.

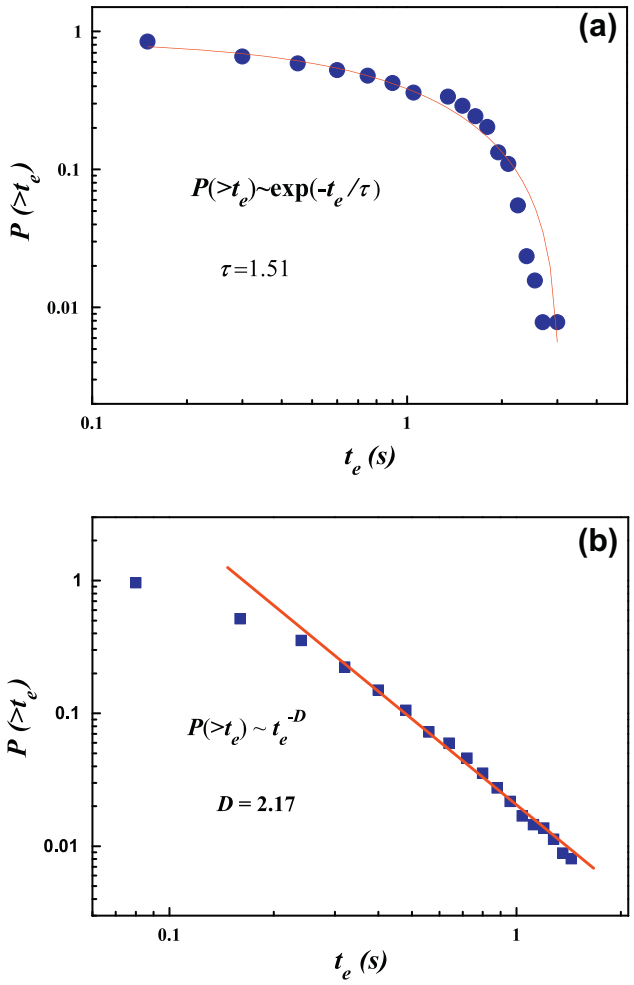

Fig. 7. Logarithmic plot of the cumulative incubation time distribution of serrations $P(>t_e)$ vs. t_e for SST (a) and MST (b), which are fitted by the Poisson distribution and the power-law distribution, respectively.

From the analysis above, one can see that the statistics of the serrated events for the MSTs is completely different from that of the MSTs. The distribution change on both the size and the incubation time of the serrated events should arise from the introduction of SBIs into the deformation process, which in turn causes a fundamental change of the stick–slip dynamics of shear bands. As can be seen from Eq. (6), the SBIs, which are a function of the displacements of all shear bands involved in the deformation, link the motions of single shear bands, thus increasing the number of degrees of freedom and rendering the dynamics more complicated compared to that captured in Eq. (3). In particular, the emergence of a power-law relation in the statistics of the serrated events in the case of the MSTs suggests that shear bands are correlated and self-organized during the deformation process. Thus, we infer that one serrated event during the MSTs may be caused by the collective operation of several shear bands.

3.4. Effect of SBI on the fracture morphology

As the sliding of shear bands will leave some shear striations in the principal shear plane, the effect of SBIs on the deformation behavior of BMG can also be reflected in the fracture morphology of the samples. As shown in Fig. 8a, the fracture surface of a typical BMG in compression is usually composed of two distinct zones: a zone with vein patterns and a smooth zone [3,57]. The vein-patterned zone usually covers most of the fracture surface and is formed in the final, catastrophic fracture process where the elastic energy of the whole sample is released in a very short time. In this stage, the temperature can reach values high enough even to cause the melting of the material [3]. In contrast, the smooth region corresponds to the stable intermittent sliding process of the dominant shear band before final fracture [8]. Thus, shear offsets or striations, associated with the stress drop in the stress–strain curves, are often observed in this region. Fig. 8b–f show typical fracture morphologies of SST and MST samples after failure. As can been from Fig. 8b and d, both MST and SST specimens display similar vein patterns, indicating a similar final fracture process along the shear plane. However, there is a significant difference in their smooth regions: striations with a regular spacing are observed for the SST sample (see Fig. 8c), while for MST samples, discontinuous, irregular striations with various step sizes are found (Fig. 8d and e).

As observed in other Zr-based BMGs, the regular striations are closely related with the regular serrations in the stress–strain curves for the SST. The average spacing of striations, Δu_s^{av}, measured from Fig. 8c, is 3.2 μm, which is consistent with the previously reported values [8,29]. By considering the machine–sample assembly, Maaß et al. [9] recently proposed a relation between the vertical shear displacement, u_{pl}^{SB}, and the load drop, ΔF:

$$u_{pl}^{SB} = \Delta F(C_M + C_S) \tag{8}$$

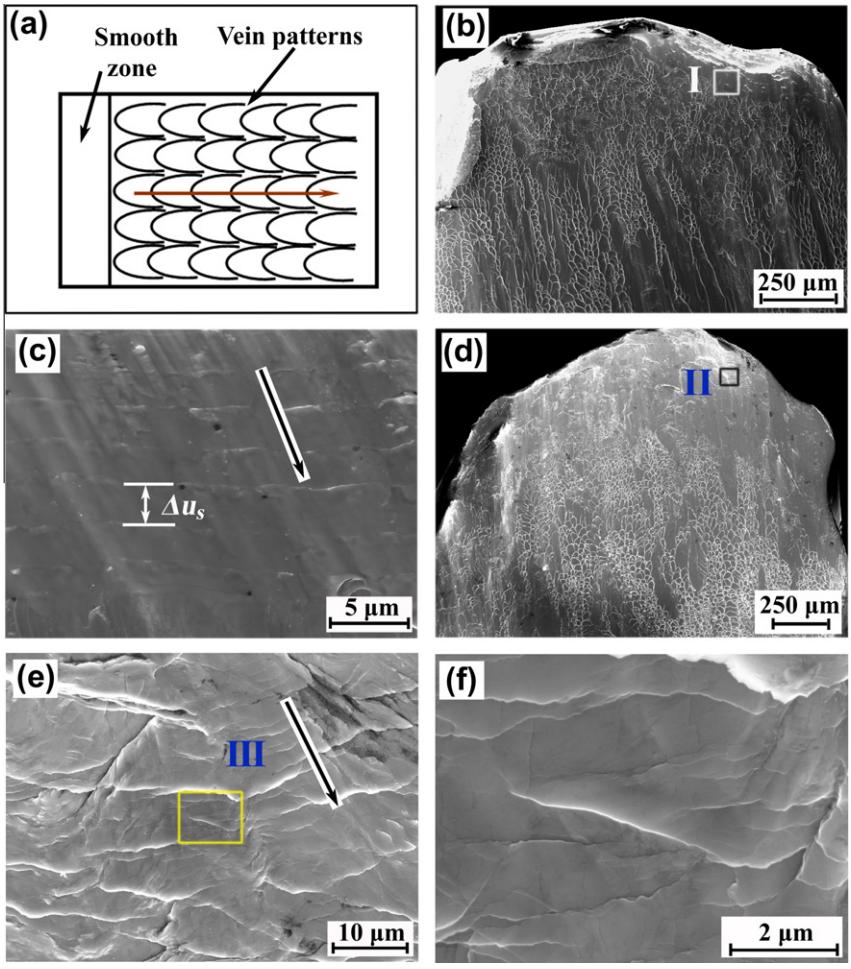

Fig. 8. (a) Typical fracture surface for metallic glasses. (b) The fracture surface for a SST sample. (c) The enlarged view of the smooth region I in (b) shows the regular striations. (d) The fracture surface for a MST sample. (e) The enlarged view of the smooth region II exhibits discontinuous, irregular striations. (f) The enlarged view of the region III in (e) displays much finer striations.

Here, C_M and C_S are the respective compliance of the machine and the sample. In our study, the value for C_S calculated from the Young's modulus E ($C_S = 4L/(\pi d^2 E)$) is 20.4 nm N^{-1} and $C_M \approx C_S$. The average load drop estimated from the stress–time curve of the SST is 60 N. Thus, according to Eq. (8), the calculated value for u_{pl}^{SB} is 3.26 μm, which is in good agreement with the value ($\Delta u_v = 2.8$ μm) estimated from the average spacing of the striations ($\Delta u_v = \Delta u_s^{av} cos\theta$ with a shear angle $\theta = 41°$). This confirms that the serrations arise from the intermittent motion of the dominant shear band. For the MST, however, there are no such characteristic shear offsets. As can be seen from Fig. 8f, many striations with much finer spacings are also observed from the enlarged view of the irregular striations in Fig. 8e. Thus, it is very difficult to estimate the average spacing of the shear offsets, suggesting that the shear banding process in the MSTs is much more complex than that in the SSTs. This furthermore verifies the statistics of the stress drops for the MSTs which can be captured by a power-law scaling. In addition, the smooth regions in the MSTs cover a much larger area than the case of the SST sample, indicating a more stable shear-band propagation and enhanced plastic deformability due to the presence of SBIs.

3.5. Correlations between the motion of shear bands in the presence of SBIs

The experimental results above suggest that the operation of multiple shear bands is correlated during one serration in the presence of SBIs. In this section, we will give a quantitative analysis of the correlation based on the numerical solution of the stick–slip model proposed in Section 3.1. From the kinetic equations, it can be seen that the only unspecified term is the internal resistance of the shear band, σ_f, which reflects the effects of intrisic material properties (such as glass structure and free volume content) on the deformation dynamics. σ_f can be described by the constitutive flow law of metallic glass, which is often a function of strain rate as well as internal variables (free volume, temperature, etc.). An example of the constitutive law is given by the shear transformation zone (STZ) theory [2,12]:

$$\tau = \tau_s - \tau_s\left[\frac{ln(\dot{\gamma}_s/\dot{\gamma})}{C_s\tau_s\Omega_s}kT\right]^{1/2} \quad (9)$$

where τ is the shear strength of the material, $\dot{\gamma}$ is the strain rate and τ_s is the thermal stress required to initiate the critical shear event with a characteristic volume Ω_s [2]. A similar expression has also recently proposed by Johnson and Samwer [14] in their cooperative shear model. However, such constitutive laws cannot be directly applied to Eq. (3) or (6), as they are not explicit forms of the strain rate. In Eq. (9), τ_s depends on the free volume, f_v, which is also a function of strain rate and shear stress: $f_v = f(\tau, \dot{\gamma})$. Furthermore, the temperature, T, may also vary with the strain rate during the deformation and hence affect the shear stress [15]. Consequently, the explicit form of $\tau(\dot{\gamma})$ is very complex and perhaps does not even exist.

Some information about σ_f can be obtained from the analysis of the stability of kinetic equations. Obviously, Eq. (3) has a steady-state solution in which the shear band slides at the loading rate v:$x_s = vt - \sigma_f(v)/k$. The stick–slip solution of shear bands or the serrated flow behavior can be regarded as a result of the instability of the steady-state solution to small perturbations. Assuming $x = x_s + \delta x(t)$, where $\delta\ x(t) = \delta x_0 exp(\lambda t)$ is the perturbation with the initial amplitude, δx_0, and inserting it into Eq. (3), we obtain $M\lambda^2 + \frac{d\sigma_f}{d\dot{x}}(v)\lambda - k = 0$. Thus, if $\frac{d\sigma_f}{d\dot{x}}(v) < 0, \lambda$ will have a positive value, i.e. the steady solution,x_s, is unstable. The same result can be also obtained from the stability analysis of Eq. (6). Thus, the sufficent condition for the appearance of serrated flow is the negative strain-rate sensitivity (SRS), $d\sigma_f/d\dot{x} < 0$. Indeed, the negative SRS of metallic glasses was experimentally observed recently by Dubach et al. [6,16], where the value of SRS changed from negative to positive when the temperature was lowered to a value at which serrations disappeared. Dubach et al. attributed the negative SRS to the existence of an additional internal variable accounting for the structural relaxation during the process of shearing [16]. In the stick–slip model proposed by Cheng et al. [15], it has been assumed that the flow stress of shear bands (σ_{f0}) is lower than its static strength (σ_y) and the difference between them provides the driving force for the slip of the shear band if the temperature rise is ignored. Here, we assume that $\sigma_f(\dot{x})$ has the form:

$$\sigma_f = \sigma_{f0} + (\sigma_y - \sigma_{f0})exp(-\dot{x}/\dot{x}_c) \quad (10)$$

where $\sigma_y = \sigma_f(0)$ is the static resistance of the shear band and the resistance exponentially decays to σ_{f0} with an increasing sliding rate, $\dot{x}$. The value of $(\sigma_y - \sigma_{f0})$ has the magnitude of the stress drop in the stress–strain curve (≈20 MPa [27,40]). $\dot{x}_c$ is the characteristic velocity, which should be in the range of the experimentally measured shear-band velocities (10^{-3}–10^{-2} ms^{-1}) [27,29] during one serration.

With Eq. (10), we solved Eqs. (3) and (6) numerically using the Runge–Kutta method. The values of parameters used for calculation are listed in Table 1. From Eqs. (2) and (5), we can see $k \approx k_1$ if S is much larger than 1. Here, we take the same value for k and k_1. During the calculation process, we also assumed that the velocity of a shear band, v_s, is always non-negative, which excludes the occurrence of small creep events (for $v_s < v$). However, this will not affect the occurrence of those truely large serrated events (for $v_s > v$) and effectively accelerate the calculation. Theoretically, the shear bands in the MST model will be activated simultaneously and operate in an exactly synchronous way for the same initial conditions of shear bands. However, in real MST experiments, some perturbations are inevitably introduced in the motions of shear bands during the deformation process due to some experimental factors such as the vibration of the testing machine and slight variation in sample parameters. We consider these effects as the small spatial inhomogeneity of the shear band velocity in the initial condition during the numerical calculation. For Eq. (6), a small initial spatial inhomogeneity of $\dot{x}$ generated by the random method is used. It is noted that the initial spatial inhomogeneity does not dominate the overall deformation response as similar numerical results are also obtained if we vary the magnitude of the initial spatial inhomogeneity or generate the homogeneity using other methods, e.g. the Gauss method. Generally, we started the system at $t = 0$. After elastic deformation for a period $t_e = \sigma_y/kv$, both systems enter the plastic deformation regime in which the serrations can be observed. The

Table 1
The values of the parameters used in the numerical solution of Eqs. (3) and (4).

v (ms^{-1})	k (GPa)	M (kg)	σ_y (MPa)	σ_{f0} (MPa)	$\dot{x}_c$ (ms^{-1})
7.5×10^{-7}	13.8	20	1600	1580	0.001

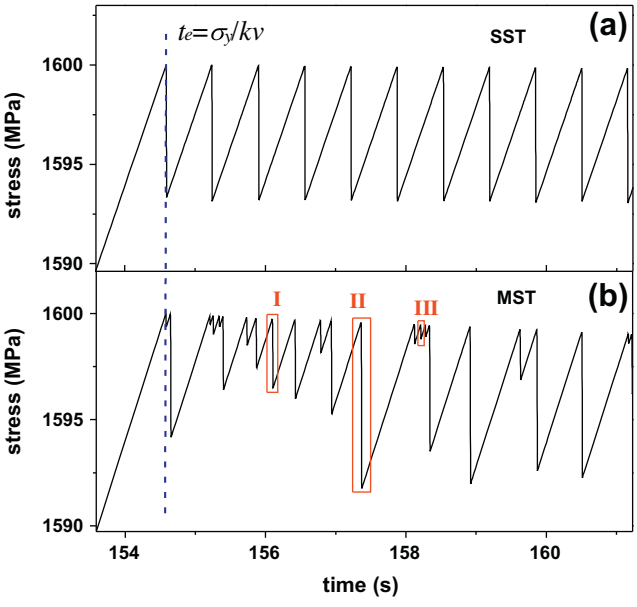

Fig. 9. Calculated stress–time curves from the numerical solution of the stick–slip models of shear bands for SST (a) and MST (b). Both curves enter the plastic deformation regime at the loading time $t_e = \sigma_y/kv$.

displacement and the velocity of the shear bands are recorded at every time step. Fig. 9 shows the calculated stress–time curves for the SSTs and the MSTs from $\sigma = k(vt - x)$ and $\sigma = k_1\left(vt - \frac{1}{5}\sum x_i\right)$, respectively. It can be seen that the serrations for the SSTs are repeated stick–slip cycles with almost the same stress drop magnitude, while the serrations for the MSTs are irregular stick–slip cycles with various sizes. The calculated stress–time curves resemble our experiments very well, suggesting that the stick–slip models in the present study capture the basic deformation process of SSTs and MSTs.

For the SSTs, the serrations correspond to periodic stick–slip motions of a single shear band (see Fig. 10a). This involves the elastic loading over a large incubation time during the "stick" phase and a rapid "slip" phase with high shear-band velocity. During the "slip" phase, the shear-band velocity first increases rapidly, reaches a maximum, then rapidly decreases to zero. The maximum velocity is determined by the values of $(\sigma_y - \sigma_{f0})$ and $\dot{x}_c$. For the MSTs, however, the situation becomes more complex. Fig. 10b shows the shear-band velocities corresponding to serrations I, II and III in Fig. 10a, respectively. As can be seen, serrations in the MSTs correspond to the collective slip motions of multiple shear bands and each can reach a different maximum velocity. The magnitude of the stress drop is determined by the maximum velocities as well as the number of participating shear bands. For the larger serrations I and II, almost all the shear bands are involved in the plastic events and their velocities (v_s) are relatively high (up to 0.0004 ms^{-1}). While for the small serration III, only two shear bands are activated and the maximum velocities they can reach are very low (about one order of magnitude lower than serration II). In any case, the motion of shear bands seems to be well organized and correlated during deformation: once a single shear band is activated, it will trigger other shear bands, and once the shear band is "stuck", other shear bands subsequently stop their motion. In addition, the whole acceleration and deceleration process is accomplished in a very short time (about 0.01 s in our simulation), which is about two order of magnitude less than the elastic loading time. Thus, the operation of multiple shear bands can be regarded as an avalanche event. All these results clearly demonstrate that the serration process corresponds to the collective stick–slip motion of multiple shear bands when a large number of shear bands are induced during deformation. This may have implications for understanding the deformation process of those ductile BMGs or their composites. Our results also verify our deduction from experimental results and give a basic picture for the operating process of multiple shear bands in metallic glasses.

The stick–slip instability has been studied extensively in a large number of laboratory friction experiments, which might be analogous to earthquake rupture, and theoretical analysis has been done to determine the nature of the instability and the conditions under which it occurs [58–60]. One important finding is that if the constitutive friction stress depends on the slip rate and some state variables (such as

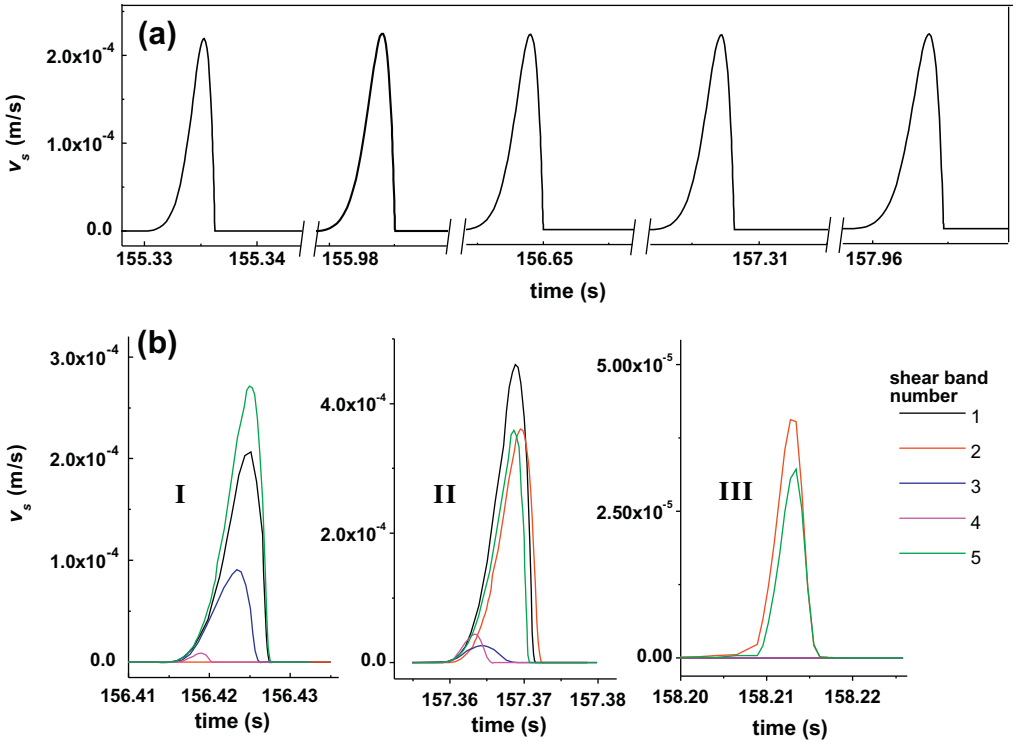

Fig. 10. (a) The calculated shear band velocity v_s for the SST with time t. (b) The calculated velocities for shear bands in the MST corresponding to serrations I, II and III in Fig. 9b.

the Ruina–Dieterich slip law [61]), the appearance of stick–slip motion is closely related to a critical spring stiffness which depends on the loading rate. When the spring stiffness is lower than the critical value, the steady-state slipping will become unstable and stick–slip motion appears. For metallic glasses, the disappearance of serrations with lowering temperature or increasing strain rate has also been reported [16,34], features which are very similar to that of rock friction. This suggests that the evolution of some state variables which describe the structural relaxation process must be considered in the stick–slip dynamics of shear bands. State variables could be the content of free volume or temperature within the shear band, which gradually evolve into their steady-state values during deformation and are responsible for the rate softening of the stress. The present constitutive law (Eq. (10)) is only a function of the instantaneous slipping rate and does not contain any memory effect of the deformation history—this is perhaps the biggest weakness of our stick–slip model: it cannot predict the disappearance of serrations at low temperatures or high strain rates. A stick–slip model with a more sophisticated constitutive law, which takes the effect of internal variables into account, is required and deserves further investigation.

4. Conclusions

We have developed a simple method in order to introduce SBIs by simultaneously compressing several BMG samples. The dynamics of shear bands and serrated flow in a Zr-based metallic glass was systematically investigated. Statistical analysis of the stress drops and incubation times of serration shows that the operation of multiple shear bands is a complex, scale-free process during which shear bands are highly correlated, compared to randomly generated, uncorrelated serrated flow events for a single shear band. The investigations of the shear plane after failure provide further evidence and insights into the deformation dynamics and corroborate the assumption of SBIs. Stick–slip models for a single shear band and multiple interacting shear bands are also proposed and numerically calculated. The results are in good agreement with experimental findings, and offer a basic understanding of the operation process of multiple shear bands and their correlation during one serration. This may help to better understanding the deformation mechanism of ductile metallic glasses or their composites.

Acknowledgments

The authors thank S. Donath, M. Frey, H. Jie, Q. Luo, Y. Zhang, K. K. Song, Z. Wang for technical assistance and stimulating discussions. This work was supported by German Science Foundation under the Leibniz Program (Grant EC 111/26-1). W.H.W. thanks the financial support from the NSF of China (Grant No. 50921091) and MOST 973 of China (2010CB731603).

References

[1] Pampillo CA. J Mater Sci 1975;10:1194.
[2] Schuh CA. Acta Mater 2007;55:4067.
[3] Chen MW. Ann Rev Mater Res 2008;38:445.
[4] Wright WJ, Saha R, Nix WD. Mater Trans JIM 2001;42:642.
[5] Klaümunzer D, Maaß R, Torre FHD, Löffler JF. Appl Phys Lett 2010;96:061901.
[6] Dubach A, Torre FHD, Löffler JF. Philos Mag Lett 2007;87:695.
[7] Torre FHD, Dubach A, Schällibaum J, Löffler JF. Acta Mater 2008;56:4635.
[8] Song SX, Bei H, Wadsworth J, Nieh TG. Intermetallics 2008;16:813.
[9] Maaß R, Klaumünzer D, Löffler J. Acta Mater 2011;59:3205.
[10] Lewandowski JJ, Greer AL. Nat Mater 2006;5:15.
[11] Spaepen F. Acta Metall 1977;25:407.
[12] Argon AS. Acta Metall 1979;27:47.
[13] Falk ML, Langer JS. Phys Rev E 1998;57:7192.
[14] Johnson WL, Samwer K. Phys Rev Lett 2005;95:195501.
[15] Cheng YQ, Han Z, Li Y, Ma E. Phys Rev B 2009;80:134115.
[16] Dubach A, Torre FHD, Löffler JF. Acta Mater 2009;57:881.
[17] Klaumünzer D, Maaß R, Löffler JF. J Mater Res 2011;26:1453.
[18] Ashby MF, Greer AL. Scr Mater 2006;54:321.
[19] Johnson WL. MRS Bull 1999;24:42.
[20] Wang WH, Dong C, Shek CH. Mater Sci Eng R 2004;44:45.
[21] Löffler JF. Intermetallics 2003;11:529.
[22] Wang WH. Adv Mater 2009;21:4524.
[23] Li J, Wang ZL, Hufnagel TC. Phys Rev B 2002;65:144201.
[24] Kim JJ, Choi Y, Suresh S, Argon AS. Science 2002;295:654.
[25] Jiang WH, Atzmon M. Acta Mater 2003;51:4095.
[26] Wright WJ, Schwarz RB, Nix WD. Mater Sci Eng A 2001;319–321:229.
[27] Song SX, Nieh TG. Intermetallics 2009;17:762.
[28] Song S, Nieh T. Intermetallics 2011. http://dx.doi.org/10.1016/j.intermet.2011.06.018.
[29] Wright WJ, Samale MW, Hufnagel TC, LeBlanc MM, Florando JN. Acta Mater 2009;57:4639.
[30] Leamy H, Wang T, Chen H. Metall Mater Trans 1972;3:699.
[31] Liu CT, Heatherly L, Horton J, Easton D, Carmichael C, Wright J, et al. Metall Mater Trans A 1998;29:1811.
[32] Bruck HA, Rosakis AJ, Johnson WL. J Mater Res 1972;3:699.
[33] Jiang MQ, Dai LH. J Mech Phys Solids 2009;57:1267.
[34] Schuh CA, Nieh TG. Acta Mater 2003;51:87.
[35] Dalla Torre FH, Dubach A, Nelson A, Löffler JF. Mater Trans 2007;48:1774.
[36] Golovin YI, Ivolgin VI, Khonik VA, Kitagawa K, Tyurin AI. Scr Mater 2001;45:947.
[37] Cheng YQ, Ma E. Prog Mater Sci 2011;56:379.
[38] Lewandowski JJ, Wang WH, Greer AL. Philos Mag Lett 2005;85:77.
[39] Tan J, Zhang Y, Sun BA, Stoica M, Li CJ, Song KK, et al. Appl Phys Lett 2011;98:151906.
[40] Han Z, Wu WF, Li Y, Wei YJ, Gao HJ. Acta Mater 2009;57:1367.
[41] Scudino S, Surreddi KB, Wang G, Eckert J. Scr Mater 2010;62:750.
[42] Wu WF, Li Y, Schuh CA. Philos Mag 2008;88:71.
[43] Das J, Tang M, Kim K, Theissmann R, Baier F, Wang W, et al. Phys Rev Lett 2005;94:205501.
[44] Sarmah R, Ananthakrishna G, Sun BA, Wang WH. Acta Mater 2011;59:4482.
[45] Sun BA, Wang WH. Appl Phys Lett 2011;98:201902.
[46] Sun BA, Yu HB, Jiao W, Bai HY, Zhao DQ, Wang WH. Phys Rev Lett 2010;105:035501.
[47] Schroers J, Johnson WL. Phys Rev Lett 2004;93:255506.
[48] Chihab K, Estrin Y, Kubin LP, Vergnol J. Scr Metall 1987;21:203.
[49] Kumar J, Ciccotti M, Ananthakrishna G. Phys Rev E 2008;77:045202.
[50] Bandyopadhyay R, Basappa G, Sood AK. Phys Rev Lett 2000;84:2022.

[51] Torre FHD, Dubach A, Siegrist ME, Löffler JF. Appl Phys Lett 2006;89:091918.
[52] Bak P, Tang C, Wiesenfeld K. Phys Rev Lett 1987;59:381.
[53] Carlson JM, Langer JS. Phys Rev Lett 1989;62:2632.
[54] Wang G, Chan KC, Xia L, Yu P, Shen J, Wang WH. Acta Mater 2009;57:6146.
[55] Sánchez R, Newman DE, Carreras BA. Phys Rev Lett 2002;88:068302.
[56] Ahrens J, Dieter U. Computing 1974;12:223.
[57] Han Z, Li Y. J Mater Res 2009;24:3620.
[58] Ruina A. J Geophys Res 1983;88:10359.
[59] Rice JR, Ruina AL. J Appl Mech 1983;50:343.
[60] Gu JC, Rice JR, Ruina AL, Tse ST. J Mech Phys Solids 1984;32:167.
[61] Ranjith K, Rice JR. J Mech Phys Solids 1999;47:1207.